Published in final edited form as:
Pharm Res. 2014 August ; 31(8): 2086–2094. doi:10.1007/s11095-014-1310-x.

Early Diagnosis of Orthopedic Implant Failure Using Macromolecular Imaging Agents

Ke Ren,
Department of Pharmaceutical Sciences, University of Nebraska Medical Center, Omaha, NE, 68198, USA

Anand Dusad,
Department of Internal Medicine/Rheumatology Division, University of Nebraska, Medical Center, Omaha, NE, 68198, USA

Yijia Zhang,
Department of Pharmaceutical Sciences, University of Nebraska Medical Center, Omaha, NE, 68198, USA

P. Edward Purdue,
Hospital for Special Surgery, New York, NY, 10021, USA

Edward V. Fehringer,
Department of Orthopaedic Surgery and Rehabilitation, University of Nebraska, Medical Center, Omaha, NE, 68198, USA

Kevin L. Garvin,
Department of Orthopaedic Surgery and Rehabilitation, University of Nebraska, Medical Center, Omaha, NE, 68198, USA

Steven R. Goldring, and
Hospital for Special Surgery, New York, NY, 10021, USA

Dong Wang[*]
Department of Pharmaceutical Sciences, University of Nebraska Medical Center, Omaha, NE, 68198, USA

Abstract

Purpose—To develop and evaluate diagnostic tools for early detection of wear particle-induced orthopaedic implant loosening.

Methods—*N*-(2-hydroxypropyl)methacrylamide (HPMA) copolymer was tagged with an near infrared dye and used to detect the inflammation induced by polymethylmethacrylate (PMMA) particles in a murine peri-implant osteolysis model. It was established by inserting implant into distal femur and with routine PMMA particles challenging. The osteolysis was evaluated by micro-CT and histological analysis at different time points.

[*]Correspondence should be addressed to Dong Wang. University of Nebraska Medical Center, 986025 Nebraska Medical Center, COP 3026, Omaha, Nebraska 68198-6025, USA. Tel.: 402-559-1995, Fax: 402-559-9543, dwang@unmc.edu.

Results—Significant peri-implant osteolysis was found three-month post PMMA particle challenge by micro-CT and histological analysis. At one-month time point, when there was no significant peri-implant bone loss, HPMA copolymer-near infrared dye conjugate was found to specifically target to the femur with PMMA particles deposition, but not the contralateral control femur with PBS infusion.

Conclusion—The results from this study demonstrated the feasibility of utilizing the macromolecular diagnostic agent to report particle-induced peri-implant inflammation prior to the development of detectable osteolysis. Recognition of this early pathological event would provide the window of opportunity for prevention of peri-implant osteolysis and subsequent orthopaedic implant failure.

Keywords

HPMA copolymer; inflammation targeting; early diagnosis; aseptic implant loosening; ELVIS

INTRODUCTION

There are almost 1.5 million joint replacement surgeries performed worldwide each year and the number is expected to increase to 4 million annually by 2030 (1, 2). Despite the great success of joint replacement surgery, the overall ten-year revision rate for total joint replacement is close to 10%. Revision surgery is often associated with a shorter duration of implant survival and poses higher risks for the patient (3, 4). Aseptic loosening is one of the major reasons limiting the longevity of the prosthetic implants (5). Inflammation caused by wear particles generated from the articulating surfaces of the prosthetic components is considered to be the major cause of aseptic implant loosening and clinical failure after joint replacement (6). Wear particles have been shown to activate macrophages and induce a granulomatous inflammatory reaction that results in osteoclast-mediated peri-implant osteolysis at the bone-implant interface, leading to the loss of the fixation and structural bone support (5, 7, 8).

To date, clinical and serial radiographic evaluations are the cornerstones in identifying implant loosening (9, 10). However, peri-implant particle-induced inflammation that leads to loosening is often a silent pathology without radiograpic changes in its early stages (11, 12). Even though pain or other symptoms are reported, current standard radiographic evaluation techniques are relatively insensitive in capturing the biological change and degree of bone loss at early stage (12, 13). Although three-dimensional computed tomography, magnetic resonance imaging and positron emission tomography have been developed for measuring osteolysis (14-16), there is still no sensitive early detection tool to identify particle-induced inflammation prior to the development of extensive osteolysis.

Recent data from our laboratories have demonstrated that *N*-(2-hydroxypropyl) methacrylamide (HPMA) copolymer selectively accumulates at sites of wear particle-induced inflammation in a murine calvarial osteolysis model. When conjugated with an imaging probe, the copolymer can effectively identify sites of particle-induced inflammation prior to the onset of osteolysis (17). Though the murine calvarial osteolysis model recapitulates many biological features of wear debris-associated osteolysis and has been

widely used (18, 19), it has many limitations. The model does not have a prosthetic implant and the prosthesis/medullar canal interaction is absent. Furthermore, the time needed to develop the model is very short, which does not reflect the chronic nature of the disease in humans. To better simulate the clinical scenario, we selected a well-established, implant-containing murine femur prosthesis failure model in the current study (20-22). By inserting a stainless steel pin into the distal femur, the pin/bone interface would be created, allowing the access of particles to the bone surface for direct interaction and subsequent gradual osteolysis. We hypothesized that the HPMA copolymer based imaging probe could passively target the sites of pathology induced by wear particles prior to incipient osteolysis and would provide a sensitive diagnostic tool for the early detection of inflammation in a model that more appropriately recapitulates the biologic events in human subjects with aseptic wear particle-induced peri-implant inflammation and loosening.

MATERIALS AND METHODS

Synthesis and characterization of HPMA copolymer conjugates

Synthesis of Poly(HPMA-co-APMA): HPMA (1 g, 6.98 mmol) (23), *N*-(3-aminopropyl)methacrylamide hydrochloride (APMA, 12.5 mg, 0.07 mmol, Polysciences, Inc., Warrington, PA), azobisisobutyronitrile (6.74 mg, 41 mol, Sigma-Aldrich, Milwaukee, WI), *S*,*S*′-bis(α,α′-dimethyl-α”-acetic acid)-trithiocarbonate (24) (6.26 mg, 23.6 mol, Sigma-Aldrich, Milwaukee, WI) and *N*-methacryloylaminopropyl fluorescein thiourea (25) (4 mg) were dissolved in 8 mL methanol, placed in an ampoule, and purged with N_2 for 5 min. The ampoule was flame-sealed and maintained at 40 °C fo r 48 h. The product was purified by LH-20 column (GE HealthCare, Piscataway, NJ) to remove the unreacted low molecular weight compounds and then lyophilized. The final yield was 0.42 g. The amine content of the copolymer was determined to be 2.7×10^{-5} mol/g using the ninhydrin assay (26). The weight average molecular weight ($M = 3.71 \times 10^4$ *w*) and number average molecular weight ($M = 2.65 \times 10^4$ *n*) of copolymers were determined based on HPMA homopolymer calibration using an ÄKTA FPLC system (GE HealthCare, Piscataway, NJ) equipped with UV and RI detectors.

Synthesis of near infrared dye 800CW-labeled HPMA copolymer (P-IRDye): Poly(HPMA-co-APMA) (16.5 mg, containing 0.00044 mmol of amine) and IRDye 800CW NHS Ester (0.5 mg, 0.00043 mmol, LI-COR® Biosciences, Lincoln, NE) were dissolved in dimethylformamide (DMF, 300 L) with *N*, *N*-diisopropylethylamine (DIPEA, 5 L) added. The solution was stirred overnight in darkness at room temperature. The product was then purified on an LH-20 column and lyophilized. The final product yield was 15.02 mg. The IRDye 800CW content was determined to be 1.1×10^{-5} mol/g using a Lambda 10 UV/Vis Spectrometer (PerkinElmer, Shelton, CT). The synthetic route is shown in Figure 1.

Murine prosthesis failure model

Poly (methyl methacrylate) (PMMA) particles (1-10 m, Bangs Laboratories, Fishers, IN) were soaked in 70 % ethanol overnight, then washed and suspended in sterile phosphate-buffered saline (PBS). A limulus assay was performed using a Pyrosate® kit (Associates of Cape Cod, Inc., East Falmouth, MA) to confirm that the treated particles were endotoxin-

free. All animal experiments were performed according to a protocol approved by University of Nebraska Medical Center Institutional Animal Care and Use Committee. Male Swiss Webster mice (10 weeks, Charles River Laboratories Inc., Wilmington, MA) were anesthetized with a mixture of xylazine and ketamine. Both legs were shaved. The surgical site and peripheral region (~ 1 cm diameter) were clipped free of hair, scrubbed twice with betadine, and then wiped with 70% isopropyl alcohol. A proximal-to-distal incision along the medial aspect of the patella was made and the patella was reflected laterally to expose the femoral condyles. A 25-gauge needle was used to manually drill through the intercondylar notch to access the medullary cavity and the marrow cavity of the femur was reamed out to a depth of 5 mm from the condyles. The medullary canal was flushed with PBS. To help induce osteolysis, 1 mg of particles in 10 μL sterile PBS was injected into the medullary canal before insertion of the pin. A 0.45 mm in diameter and 5 mm in length stainless steel pin was then inserted into the medullary chamber of the distal femur. The patella was reduced to its correct anatomical position. The wound was then cleaned, rinsed with saline with antibiotics (100 U/mL penicillin and 100 mg/mL streptomycin) and closed by sutures in layers. For the contralateral control femur, the same surgery was performed. The only difference was that PBS without particles was injected. Twice daily antibiotic (cefazolin sodium, 25mg/kg, oral) and analgesia drug (buprenorphine, 0.5mg/kg, s.c.) were given for three days following surgery. The mice were then scanned with X-rays to verify implant position. Intra-articular injections of PMMA particles (1 mg in 10 μL PBS) were performed twice a month on the side with the initial PMMA deposition. For the contralateral control side, PBS without particles was administered.

Near Infrared Optical Imaging

One-month post surgery, 0.3 mg P-IRDye was administered to each mouse via tail vein injection. Optical imaging using a Pearl® Impulse small animal imaging system (LI-COR, Lincoln, NE) was performed daily after injection to evaluate the distribution of the HPMA copolymer-based imaging probe. The near-infrared signal intensity was measured from a consistent region of interest at the femur site for all the mice. The signal intensity was quantitatively analyzed by resident software. The signal is calculated by the following equation: Signal = total intensity for ROI of interest – (background mean intensity × area for ROI of interest).

Micro-computerized tomography (micro-CT) analyses

Mice were euthanized in a carbon dioxide chamber at one, two or three months after surgery. The femurs were retrieved and stored in 70 % ethanol and then scanned using a high-resolution micro-CT (Skyscan 1172, Skyscan, Aartselaar, Belgium) for qualitative and quantitative analyses. The X-ray source was set at a voltage of 70 kV and a current of 141 A with a fixed exposure time of 480 ms. Eight frames were averaged with a rotation step of 0.7° following an angle of 180°. The resolution was 5.5 m using medium camera pixel size (2000 × 1336) with a 0.5 mm Al filter. Micro-CT analysis focused on the distal femur wherein a volume of interest (VOI) of 100 slides was selected distally from 300 slices above the growth plate. The region of interest (ROI) within the VOI was defined as a ring from the implant axis with a radius of 0.6 mm. The pin was excluded from the ROI by adjusting the setting thresholds, which were kept constant for all the samples. Setting the optimized

parameters minimized the artifacts. Three-dimensional reconstructions of the scanned region by the system reconstruction software (NRecon, Skyscan) and bone background segmentation were then performed. For quantitative analysis of the particle-induced osteolysis, the resident software (CTAn, Skyscan) was used to obtain specific morphometric parameters within the ROI, including bone volume (BV), tissue volume (TV), percent bone volume (BV/TV), bone surface density (BS/TV), intersection surface (i.S), and structural thickness of bone in 3D. In the two-dimensional (2D) slice-by-slice analysis, we calculated average bone fragment areas, average number of bone fragments and mean polar moment of inertia (MMI). The mean bone fragment area and mean number of bone fragments stated the number and size of disconnected structure in the trabecular mesh due to resorptive activities. To produce a visual representation of the results, 3D images of the femur/implant interface were developed using the resident CT-Vol software. Methods to calculate the above mentioned 2D and 3D bone parameters are described in detail on the Skyscan website.

Histological evaluation

The femurs were fixed in 4 % neutralized paraformaldehyde for 48 h and then decalcified in 10 % EDTA with 0.5 % paraformaldehyde in PBS. The specimens were then paraffin-embedded and sectioned at a thickness of 6 μm. The sections were stained with hematoxylin and eosin (H&E) to examine the bone loss around the prosthetic pin and to evaluate debris-associated inflammation. For identification of osteoclasts, paraffin sections were tartrate-resistant acid phosphatase (TRAP) stained using a commercial staining kit (387A, Sigma-Aldrich, St. Louis, MO) according to the protocol provided by Sigma. Purple red-stained cells were identified as TRAP-positive osteoclasts. To examine the bone collagen loss, modified trichrome staining was performed as previously described (22, 27). Bone collagen stained dark blue, with color density proportional to collagen content. All the stained sections were examined with an Olympus BX51 microscope (Olympus, Japan). The region of interest for histology analysis was corresponding to the same region where micro-CT analysis was performed.

Statistical Analysis

Comparisons between the two groups for the imaging studies were evaluated with Student's t-test: two-sample two-tails assuming equal variances. Data were expressed as mean ± standard deviation. $P < 0.05$ was considered as statistically significant.

RESULTS

Surgical outcomes

A stainless steel pin was implanted into the femur. X-ray scanning verified that the pin was properly positioned in the femur (Figure 2). All of the animals tolerated the surgical procedure well and were able to ambulate with the implant within 2 days of surgery. Particle injection had no detectible influence on the normal activities of the animals.

Near-infrared optical imaging study

A strong near-infrared signal from P-IRDye was observed at the PMMA particle deposition site one-month post surgery compared with the contralateral side injected with PBS (Figure

3). Daily imaging demonstrated the persistence of the P-IRDye signal for more than 6 days. Quantitative analysis of the near-infrared signal intensity confirmed that at 6 days post P-IRDye administration, ~50 % of the signal remained, consistent with retention of P-IRDye at the PMMA particle implantation site. The distribution and retention of the P-IRDye was significantly lower in the PBS control side compared to the PMMA-challenged side ($P < 0.05$).

Micro-CT evaluation

There was a gradual decrease in peri-implant bone quantity and quality in the PMMA-challenged femur. The volume of interest for micro-CT analysis and the parameters are shown in Figure 4, and representative reconstructed 3D images of the periprosthetic bone from both groups at one, two and three months after surgery are shown in Figure 5. 3D analysis revealed lower mean BV/TV, BS/TV, i.S, and bone structure thickness in the PMMA-challenged femurs compared to PBS-treated femurs at three months post surgery (Figure 4B). As compared to the PBS control femur, the PMMA-challenged femur showed a significantly lower MMI, mean bone fragment area and a higher mean number of bone fragments in slice-by-slice 2D analysis at three months after surgery. No significant differences between PBS and PMMA-infused femurs were detected at one and two months post surgery. Taken together, both 2D and 3D micro-CT analyses show that PMMA particles induced periprosthetic bone resorption over time with clear osteolysis detectable three months after surgery, but not at one and two months.

Histological analyses

Trichrome staining demonstrated that bone collagen was well preserved in the PBS treated group (Figure 6A), whereas in the PMMA group, there were indications of significant bone collagen loss (Figure 6E) three months after surgery. H&E staining showed that the implantation of the pin without particle challenge resulted in irregular new bone formation without significant bone loss or inflammation (Figure 6B). However, femurs treated with the implant and particles showed the presence of inflammatory cell infiltration and osteolysis (Figure 6F). As shown in Figure 6G and 6H, multiple TRAP-positive cells (arrow indicated) were present on the bone surfaces in PMMA particle-challenged femurs, consistent with active osteoclast-mediated bone resorption. In contrast, TRAP-positive cells in PBS-injected femurs were detected in much lower numbers (Figure 6C, D).

DISCUSSION

Wear debris induced aseptic implant loosening is the single most important cause of long term total joint replacement failure (6). Wear particles have been shown to activate macrophages and induce a granulomatous inflammatory reaction that results in osteoclast-mediated peri-implant osteolysis at the bone-implant interface leading to loss of fixation and structural bone support (5, 28, 29). Non-invasive imaging modalities such as successive X-ray and CT have been used for the clinical diagnosis of osteolysis and implant loosening (30). These methods are effective in detecting osteolysis and associated loss of implant fixation. At early stages of osteolysis, however, the skeletal changes are minimal, and are below the detection sensitivity of these radiographic imaging techniques. Frequently, by the

time clinical symptoms are reported, considerable bone loss has already occurred, and unfortunately this bone loss is irreversible. Therefore, an urgent unmet clinical need exists to detect the early stages of wear particle-induced inflammation prior to the development of peri-implant osteolysis and implant loosening. Detection of this process at an early stage would provide an opportunity to initiate therapeutic interventions to reduce the inflammatory process and inhibit bone resorption. The present study was undertaken with the goal of developing a diagnostic tool for the early detection of prosthetic wear particle-induced peri-implant inflammation.

A few mouse models of orthopaedic wear particle-induced inflammatory osteolysis have been developed and widely used (19, 22, 31). Not every one of them can accurately recapitulate the gradual development of bone loss around prosthetic implants as seen in the human disease. In this study, we have selected a mouse model in which osteolysis is induced by introduction of PMMA (major composition of bone cement) particles into the mouse femur following implantation of a stainless steel pin. Importantly, this model results in progressive bone loss over an extended period of time, with osteolysis only becoming apparent three months after the initial inflammatory process is initiated by the particles. This model therefore provides an optimal system for the evaluation of strategies for detection of early inflammation prior to the development of overt bone loss.

As a tool for the detection of particle-induced inflammation, we conjugated an optical imaging probe to HPMA copolymers. We have recently developed such conjugates as sensitive inflammation reporters *in vivo*, based on the unique passive targeting and retention of colloids (including water-soluble polymers) at the inflammatory site (17, 32). The mechanisms were termed as **E**xtravasation through **L**eaky **V**asculature and **I**nflammatory cell-mediated **S**equestration, or ‘ELVIS’ (33). To identify inflammation prior to the development of osteolysis, we administrated the near infrared dye-labeled HPMA copolymer by tail vein injection one month after surgery, well before evidence of osteolysis. A strong near-infrared signal from the P-IRDye was observed in PMMA-particle deposited femur, whereas the contralateral side without particle challenge did not show preferential signal localization. Furthermore, P-IRDye was detectable for several days following localization to the femur, consistent with enhanced retention mechanisms. Contrary to the observation with P-IRDye, however, dose equivalent free near-infrared dye did not show any specific tissue uptake (Supplementary Figure 2). Similar results were also obtained at two and three month time points (Supplementary Figure 3 and 4). Earlier time points (one to three weeks post surgery) resulted in strong near-infrared signals on both sides, presumably as a result of the trauma and inflammation caused by surgery and pin implantation. This is in agreement with literature (34) that acute inflammation following femoral bone marrow ablation surgery generally resolved by two weeks, with complete resolution by four weeks. Together, these data indicate that HPMA based copolymers represent a sensitive tool for detection of early inflammatory osteolysis that begins after surgical healing but well in advance of detectable bone loss.

Histological analysis (H&E, TRAP and modified trichrome staining) identified bone loss in PMMA-infused femurs with increased osteoclast-like TRAP positive cells at three months post-surgery, but not at one or two months, which is consistent with the significant changes

in micro-CT parameters at these time points. Previous studies have documented the utility of micro-CT in assessing peri-implant bone architecture in models of wear particle-induced osteolysis (22, 35). In our studies, osteolysis was associated with an increase in the mean number of bone fragments and a subsequent decrease in average bone fragment area. A completely disconnected trabecular (not connected to any nearby trabecular in any direction) is marked as a fragment by the software. The changes observed with these parameters represented a more disconnected trabecular structure around the implant with potentially reduced mechanical properties (36). This disconnected and fragmented bone structure resulted in a loss of intersection surface between the bone and the implant, contributing to loss of implant fixation. The peri-implant bone loss may also lead to a decrease in the efficiency of the bone tissue to resist torsion, as evidenced by the decrease in moment of inertia (MMI) values (37). Though we believe the osteoclast-mediated bone resorption is the major driving force for the observed difference between the PMMA deposited and PBS control groups in the study, without bone dynamic data, we cannot exclude the contribution of the local bone formation and turnover rates.

Collectively, these data validate the ability of the HPMA copolymer-based macromolecular probes to detect early pathological inflammatory processes prior to the development of radiographic evidence of osteolysis. Owing to the poor tissue penetration of near-infrared imaging signals (especially through mineralized tissues) (38, 39), its clinical application in human subjects is limited. To address this and extend the clinical relevance of these findings, we labeled the HPMA copolymer with ^{125}I using a standard chloramine-T assay to further explore the imaging capability using an alternate clinical imaging modality (Supplementary Figure 6) (40). The reconstructed SPECT/CT movie showed the preferential accumulation of the imaging agent to the site with the PMMA particle injection (supplementary video 1 and 2). Clearly, this technology could be extended to other radioisotopes (such as ^{111}In, ^{99m}Tc, ^{18}F, ^{64}Cu) and other imaging modalities (such as PET/CT) that are already in clinical use for human subjects.

CONCLUSION

Using a murine femur prosthesis failure model, we showed that imaging agents based on HPMA copolymers could detect particle-induced inflammation prior to the development of anatomically detectible bone loss. Further adaptation of this system with high-energy radioisotopes may allow this nanotechnology to be used for early diagnosis of orthopaedic implant loosening in clinical settings. Importantly, the ability to identify ongoing subclinical pathology and to predict future implant failure offers a unique opportunity for preventive interventions, which may significantly prolong the lifetime of orthopaedic implants and improve the long-term outcome of total joint replacement surgery.

Supplementary Material

Refer to Web version on PubMed Central for supplementary material.

Acknowledgments

This study was supported in part by NIH/NIAMS R01 AR053325 and R01 AR062680 to D.W. and an ACR-REF: Within Our Reach Grant to S.R.G. The authors would like to thank Ms. Laura Weber for proof-reading the manuscript.

ABBREVIATIONS

HPMA	*N*-(2-hydroxypropyl)methacrylamide
APMA	*N*-(3-aminopropyl)methacrylamide
P-IRDye	HPMA copolymer-near infrared dye conjugate
PBS	Phosphate buffered saline
PMMA	Poly (methyl methacrylate)
VOI	Volume of interest
ROI	Region of interest
BV	Bone volume
TV	Tissue volume
BV/TV	Bone volume/tissue volume
BS/TV	Bone surface density
i.S	Intersection surface
MMI	Mean polar moment of inertia
H&E	Hematoxylin and eosin
TRAP	Tartrate-resistant acid phosphatase
ELVIS	Extravasation through Leaky Vasculature and Inflammatory cell-mediated Sequestration

REFERENCES

1. Teeny SM, York SC, Mesko JW, Rea RE. Long-term follow-up care recommendations after total hip and knee arthroplasty: results of the American Association of Hip and Knee Surgeons' member survey. The Journal of arthroplasty. 2003; 18(8):954–962. [PubMed: 14658097]
2. Kurtz S, Ong K, Lau E, Mowat F, Halpern M. Projections of primary and revision hip and knee arthroplasty in the United States from 2005 to 2030. The Journal of bone and joint surgery American volume. 2007; 89(4):780–785. [PubMed: 17403800]
3. Meijer MF, Reininga IH, Boerboom AL, Stevens M, Bulstra SK. Poorer survival after a primary implant during revision total knee arthroplasty. International orthopaedics. 2013; 37(3):415–419. [PubMed: 23263508]
4. Amstutz HC, Campbell P, Kossovsky N, Clarke IC. Mechanism and clinical significance of wear debris-induced osteolysis. Clinical orthopaedics and related research. 1992; (276):7–18. [PubMed: 1537177]
5. Hallab NJ, Jacobs JJ. Biologic effects of implant debris. Bulletin of the NYU hospital for joint diseases. 2009; 67(2):182–188. [PubMed: 19583551]
6. Holt G, Murnaghan C, Reilly J, Meek RM. The biology of aseptic osteolysis. Clinical orthopaedics and related research. 2007; 460:240–252. [PubMed: 17620815]

7. Purdue PE, Koulouvaris P, Potter HG, Nestor BJ, Sculco TP. The cellular and molecular biology of periprosthetic osteolysis. Clinical orthopaedics and related research. 2007; 454:251–261. [PubMed: 16980902]
8. Ingham E, Fisher J. The role of macrophages in osteolysis of total joint replacement. Biomaterials. 2005; 26(11):1271–1286. [PubMed: 15475057]
9. Stulberg BN, Della Valle AG. What are the guidelines for the surgical and nonsurgical treatment of periprosthetic osteolysis? The Journal of the American Academy of Orthopaedic Surgeons. 2008; (16 Suppl 1):S20–25. [PubMed: 18612009]
10. Talmo CT, Shanbhag AS, Rubash HE. Nonsurgical management of osteolysis: challenges and opportunities. Clinical orthopaedics and related research. 2006; 453:254–264. [PubMed: 17016218]
11. Malchau H, Potter HG. How are wear-related problems diagnosed and what forms of surveillance are necessary? The Journal of the American Academy of Orthopaedic Surgeons. 2008; (16 Suppl 1):S14–19. [PubMed: 18612008]
12. Beck RT, Illingworth KD, Saleh KJ. Review of periprosthetic osteolysis in total joint arthroplasty: an emphasis on host factors and future directions. Journal of orthopaedic research: official publication of the Orthopaedic Research Society. 2012; 30(4):546.
13. Saleh KJ, Thongtrangan I, Schwarz EM. Osteolysis: medical and surgical approaches. Clinical orthopaedics and related research. 2004; (427):138–147. [PubMed: 15552150]
14. Potter HG, Nestor BJ, Sofka CM, Ho ST, Peters LE, Salvati EA. Magnetic resonance imaging after total hip arthroplasty: evaluation of periprosthetic soft tissue. The Journal of bone and joint surgery American volume. 2004; 86-A(9):1947–1954. [PubMed: 15342757]
15. Looney RJ, Boyd A, Totterman S, Seo GS, Tamez-Pena J, Campbell D, Novotny L, Olcott C, Martell J, Hayes FA, O'Keefe RJ, Schwarz EM. Volumetric computerized tomography as a measurement of periprosthetic acetabular osteolysis and its correlation with wear. Arthritis research. 2002; 4(1):59–63. [PubMed: 11879538]
16. Puri L, Wixson RL, Stern SH, Kohli J, Hendrix RW, Stulberg SD. Use of helical computed tomography for the assessment of acetabular osteolysis after total hip arthroplasty. The Journal of bone and joint surgery American volume. 2002; 84-A(4):609–614. [PubMed: 11940623]
17. Ren K, Purdue PE, Burton L, Quan LD, Fehringer EV, Thiele GM, Goldring SR, Wang D. Early detection and treatment of wear particle-induced inflammation and bone loss in a mouse calvarial osteolysis model using HPMA copolymer conjugates. Molecular pharmaceutics. 2011; 8(4):1043–1051. [PubMed: 21438611]
18. Rao AJ, Nich C, Dhulipala LS, Gibon E, Valladares R, Zwingenberger S, Smith RL, Goodman SB. Local effect of IL-4 delivery on polyethylene particle induced osteolysis in the murine calvarium. Journal of biomedical materials research Part A. 2012
19. Zhang X, Morham SG, Langenbach R, Young DA, Xing L, Boyce BF, Puzas EJ, Rosier RN, O'Keefe RJ, Schwarz EM. Evidence for a direct role of cyclo-oxygenase 2 in implant wear debris-induced osteolysis. Journal of bone and mineral research: the official journal of the American Society for Bone and Mineral Research. 2001; 16(4):660–670.
20. Yang SY, Yu H, Gong W, Wu B, Mayton L, Costello R, Wooley PH. Murine model of prosthesis failure for the long-term study of aseptic loosening. Journal of orthopaedic research: official publication of the Orthopaedic Research Society. 2007; 25(5):603–611. [PubMed: 17278141]
21. Epstein NJ, Warme BA, Spanogle J, Ma T, Bragg B, Smith RL, Goodman SB. Interleukin-1 modulates periprosthetic tissue formation in an intramedullary model of particle-induced inflammation. Journal of orthopaedic research: official publication of the Orthopaedic Research Society. 2005; 23(3):501–510. [PubMed: 15885468]
22. Zhang T, Yu H, Gong W, Zhang L, Jia T, Wooley PH, Yang SY. The effect of osteoprotegerin gene modification on wear debris-induced osteolysis in a murine model of knee prosthesis failure. Biomaterials. 2009; 30(30):6102–6108. [PubMed: 19665222]
23. Kopeček J, B H. Poly[N-(2-hydroxypropyl)methacrylamide]—I. Radical polymerization and copolymerization European Polymer Journal. 1973; 9(1):7–14.
24. Lai JT, F D, Shea R. Functional Polymers from Novel Carboxyl-Terminated Trithiocarbonates as Highly Efficient RAFT Agents. Macromolecules. 2002; 35(18):6754–6756.

25. Omelyanenko V, Kopeckova P, Gentry C, Kopecek J. Targetable HPMA copolymer-adriamycin conjugates. Recognition, internalization, and subcellular fate. Journal of controlled release: official journal of the Controlled Release Society. 1998; 53(1-3):25–37. [PubMed: 9741911]
26. A modified ninhydrin reagent for the photometric determination of amino acids and related compounds. J Biol Chem. 1954; 211(2):907–913. WH MSaS. J. Biol. Chem. 211. [PubMed: 13221596]
27. Yang SY, Mayton L, Wu B, Goater JJ, Schwarz EM, Wooley PH. Adeno-associated virus-mediated osteoprotegerin gene transfer protects against particulate polyethylene-induced osteolysis in a murine model. Arthritis and rheumatism. 2002; 46(9):2514–2523. [PubMed: 12355500]
28. Noordin S, Masri B. Periprosthetic osteolysis: genetics, mechanisms and potential therapeutic interventions. Canadian journal of surgery Journal canadien de chirurgie. 2012; 55(6):408–417. [PubMed: 22992398]
29. Revell PA. The combined role of wear particles, macrophages and lymphocytes in the loosening of total joint prostheses. Journal of the Royal Society, Interface / the Royal Society. 2008; 5(28): 1263–1278.
30. Leopold SS, Rosenberg AG, Bhatt RD, Sheinkop MB, Quigley LR, Galante JO. Cementless acetabular revision. Evaluation at an average of 10.5 years. Clinical orthopaedics and related research. 1999; (369):179–186. [PubMed: 10611873]
31. Ren W, Wu B, Peng X, Hua J, Hao HN, Wooley PH. Implant wear induces inflammation, but not osteoclastic bone resorption, in RANK(-/-) mice. Journal of orthopaedic research: official publication of the Orthopaedic Research Society. 2006; 24(8):1575–1586. [PubMed: 16779834]
32. Quan LD, Purdue PE, Liu XM, Boska MD, Lele SM, Thiele GM, Mikuls TR, Dou H, Goldring SR, Wang D. Development of a macromolecular prodrug for the treatment of inflammatory arthritis: mechanisms involved in arthrotropism and sustained therapeutic efficacy. Arthritis research & therapy. 2010; 12(5):R170. [PubMed: 20836843]
33. Yuan F, Quan LD, Cui L, Goldring SR, Wang D. Development of macromolecular prodrug for rheumatoid arthritis. Advanced drug delivery reviews. 2012; 64(12):1205–1219. [PubMed: 22433784]
34. Shimizu T, Mehdi R, Yoshimura Y, Yoshikawa H, Nomura S, Miyazono K, Takaoka K. Sequential expression of bone morphogenetic protein, tumor necrosis factor, and their receptors in bone-forming reaction after mouse femoral marrow ablation. Bone. 1998; 23(2):127–133. [PubMed: 9701471]
35. Ma T, Huang Z, Ren PG, McCally R, Lindsey D, Smith RL, Goodman SB. An in vivo murine model of continuous intramedullary infusion of polyethylene particles. Biomaterials. 2008; 29(27): 3738–3742. [PubMed: 18561997]
36. Vermeirsch H, Nuydens RM, Salmon PL, Meert TF. Bone cancer pain model in mice: evaluation of pain behavior, bone destruction and morphine sensitivity. Pharmacology, biochemistry, and behavior. 2004; 79(2):243–251.
37. Bellido M, Lugo L, Roman-Blas JA, Castaneda S, Caeiro JR, Dapia S, Calvo E, Largo R, Herrero-Beaumont G. Subchondral bone microstructural damage by increased remodelling aggravates experimental osteoarthritis preceded by osteoporosis. Arthritis research & therapy. 2010; 12(4):R152. [PubMed: 20678201]
38. Kolari PJ, Airaksinen O. Poor penetration of infra-red and helium neon low power laser light into the dermal tissue. Acupuncture & electro-therapeutics research. 1993; 18(1):17–21. [PubMed: 8098894]
39. Mancini DM, Bolinger L, Li H, Kendrick K, Chance B, Wilson JR. Validation of near-infrared spectroscopy in humans. J Appl Physiol. 1994; 77(6):2740–2747. [PubMed: 7896615]
40. Quan LD, Yuan F, Liu XM, Huang JG, Alnouti Y, Wang D. Pharmacokinetic and biodistribution studies of N-(2-hydroxypropyl)methacrylamide copolymer-dexamethasone conjugates in adjuvant-induced arthritis rat model. Molecular pharmaceutics. 2010; 7(4):1041–1049. [PubMed: 20557133]

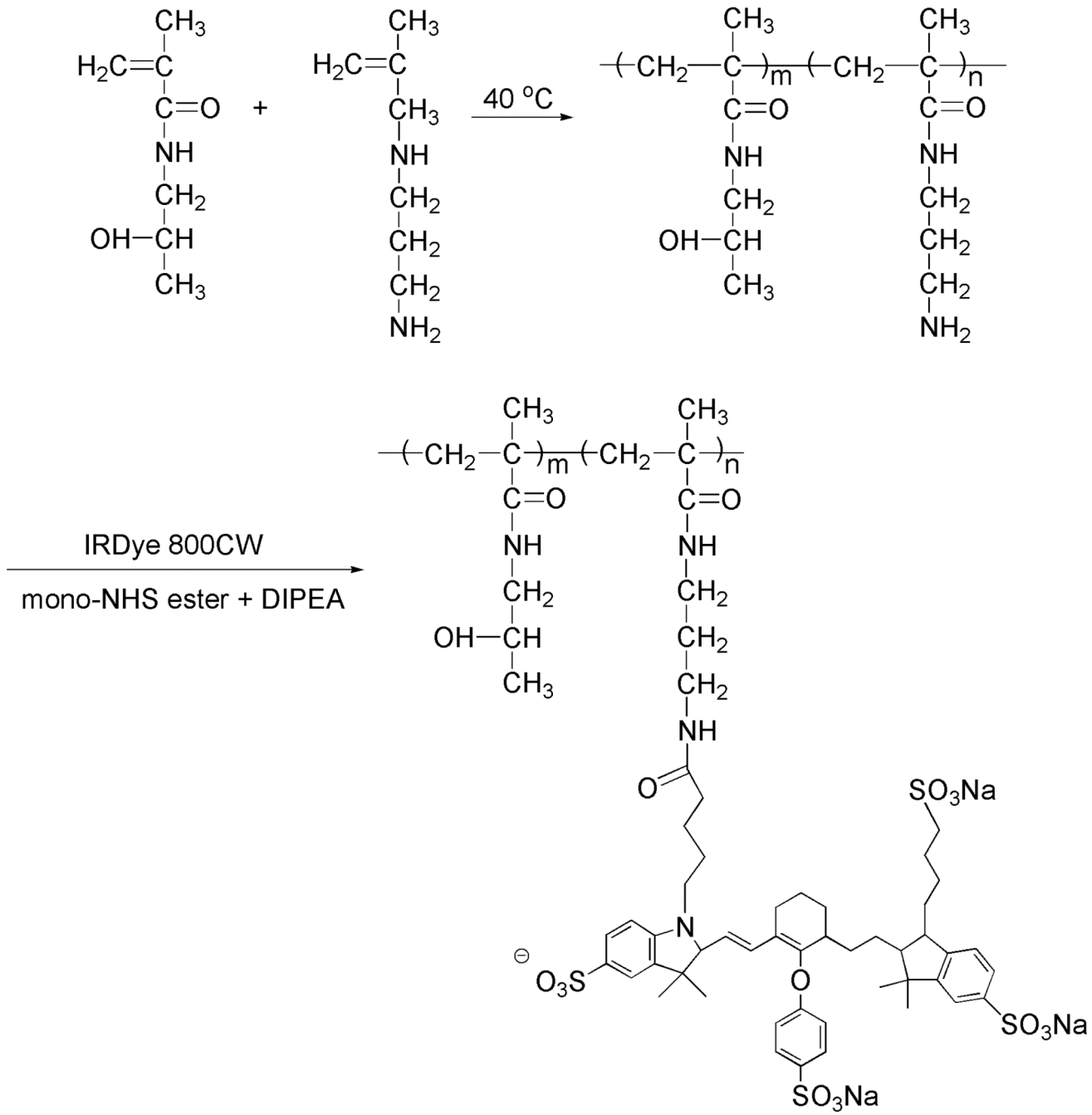

Figure 1.
The synthesis of P-IRDye.

Figure 2.
Radiograph showing the position of the pin. (A) A stainless steel pin was inserted into the distal end of the femur. (B) A radiograph taken after the femur was harvested providing a closer view of the position of the pin.

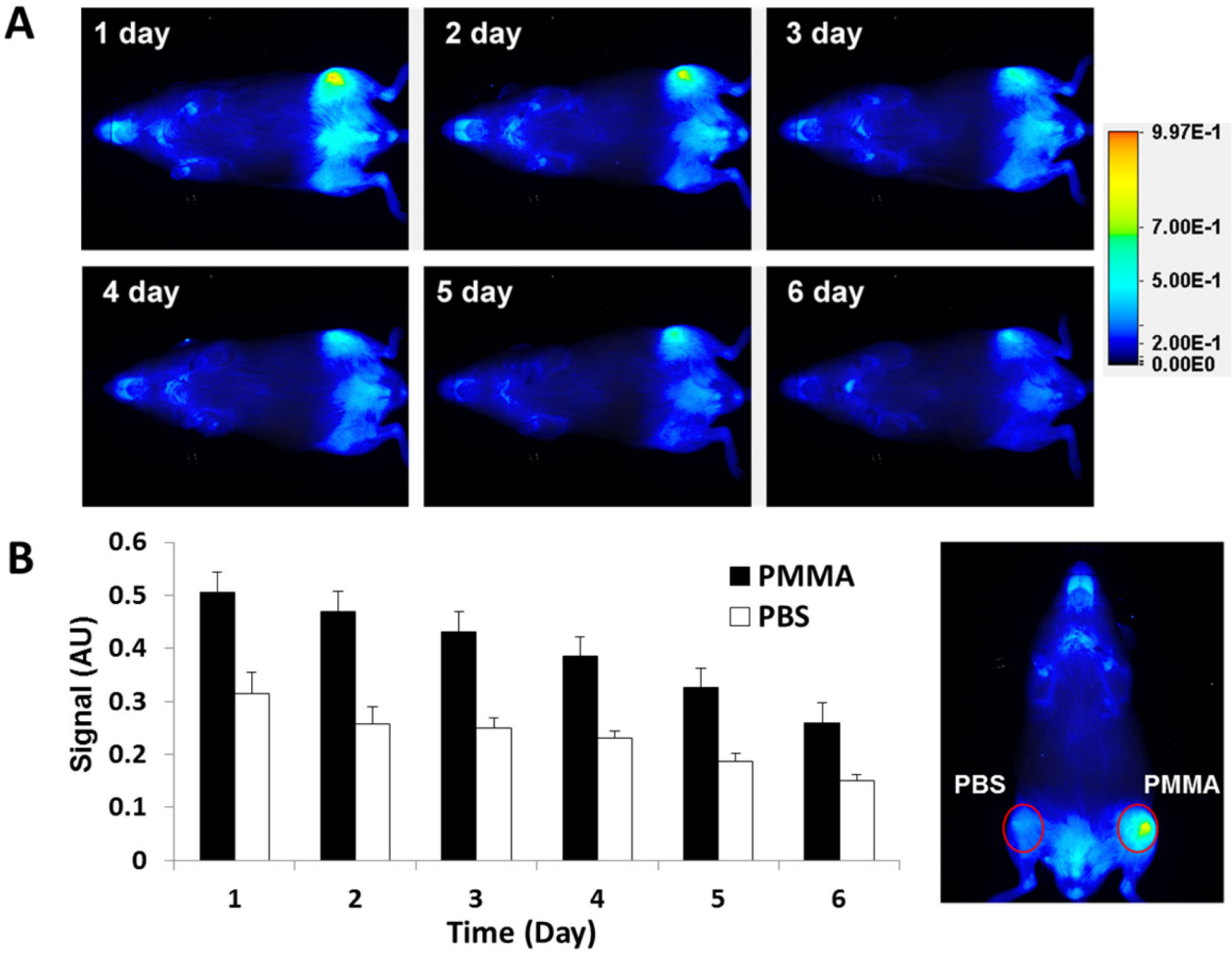

Figure 3.

Live optical imaging after PBS or PMMA challenge. P-IRDye was given via tail vein injection one month after surgery. The mice (n = 10) were imaged daily after the administration of the optical imaging agent. (A) Compared to the PBS-treated contralateral side (lower femur), the PMMA particle-challenged side (upper femur) demonstrated more intense and longer lasting near-infrared signals in the distal femur region where the PMMA particles were deposited. (B) The near-infrared signal intensity was measured from a consistent region of interest (red circle) in the femur site for all the mice. The signal intensity differences between the two sides were statistically significant ($P < 0.05$).

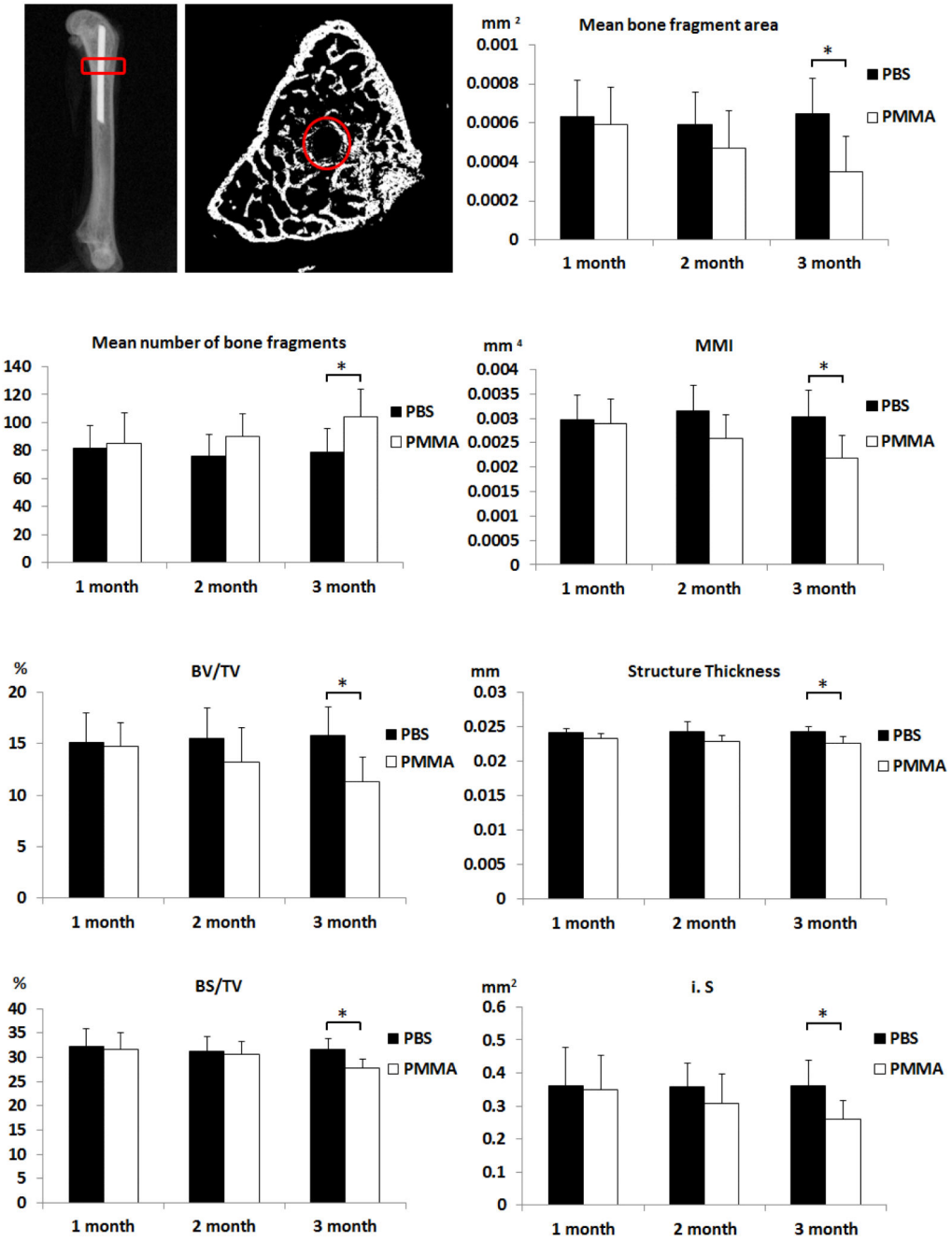

Figure 4.

Parameters of the harvested femurs measured by micro-CT. Sagittal and transverse views of representative femurs are shown. Red rectangles and circles indicate the volume of interest and region of interest, respectively, for the micro-CT analyses. 2D and 3D parameters from micro-CT analyses indicate that injection of PMMA particles led to a significant decrease of average bone fragment area, mean polar moment of inertia (MMI), percent bone volume (BV/TV), bone surface density (BS/TV), intersection surface (i.S) and structural thickness,

but increased mean number of bone fragments when compared to the contralateral PBS-treated side three months after surgery (* $P<0.05$).

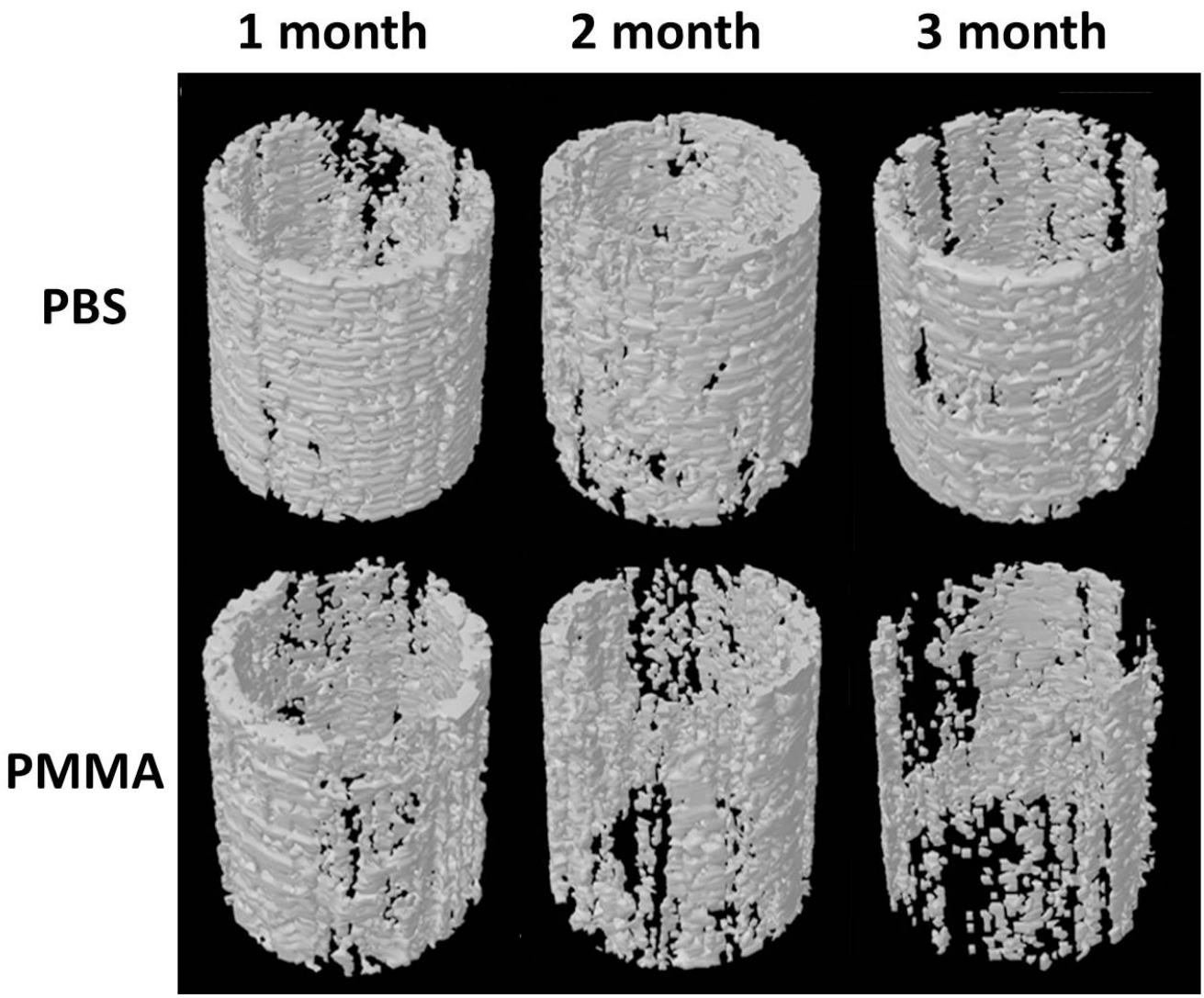

Figure 5.

Representative micro-CT reconstructed images of regions of interest in the mouse femurs at 1, 2 and 3 months after surgery. There was significant osteolysis in PMMA particle challenged femurs three months after surgery.

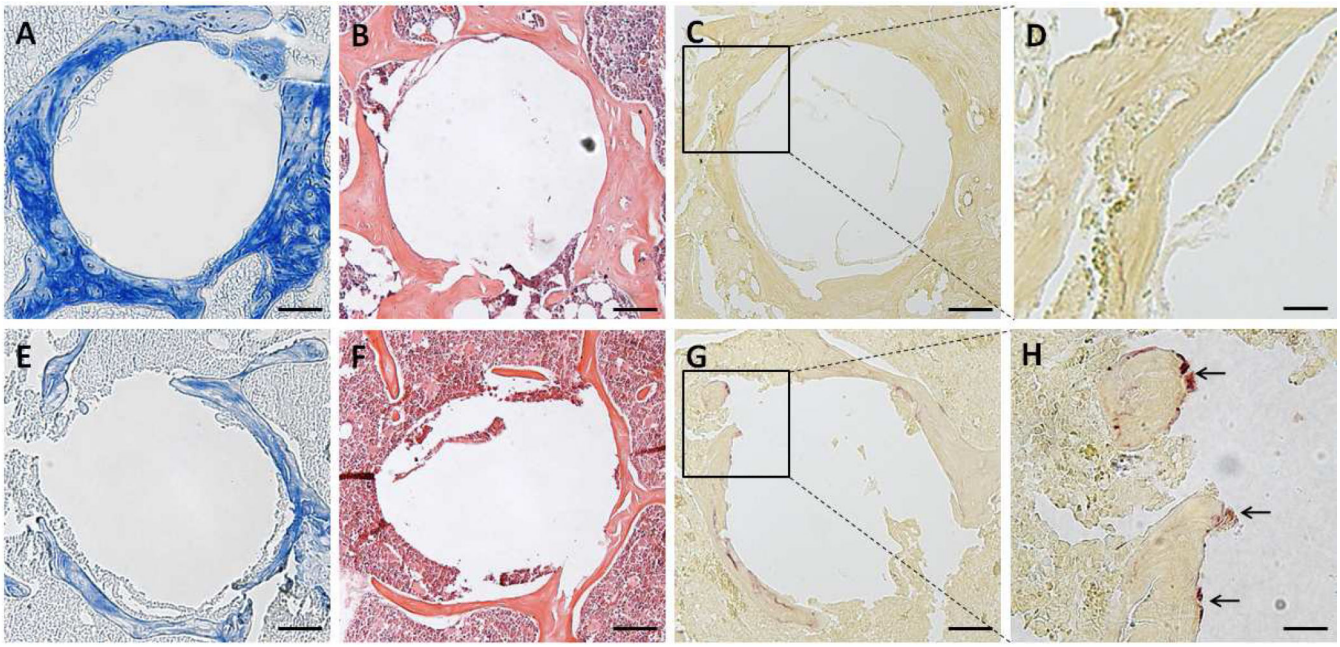

Figure 6.

Representative photomicrographs of pin-implanted femurs three months after surgery using modified trichrome (A&E), H&E (B&F) or TRAP (C, D, G, H) staining. Panels A, B and C were from femurs injected with PBS, while E, F and G were from femurs challenged with PMMA particles, bars = 100 um. Panels D and H represent the enlarged square from C and G, respectively. The arrows in panel G indicate the TRAP-positive cells. Bars = 300 um in panel D and H.